Journal of Hydroscience and Hydraulic Engineering
Vol. 28, No.2 November, 2010, 1-13

3-D NUMERICAL SIMULATION OF FLOW IN CURVED CHANNEL WITH SMALL WIDTH-TO-DEPTH RATIO FOR DUNE DEVELOPING

By

Yuki Kajikawa and Osamu Hinokidani

Graduate school of Engineering, Tottori University
Minami 4-101, Koyama-cho, Tottori 680-8552, Japan

SYNOPSIS

In a curved river with a small width-to-depth ratio, inner side scour and outer side local scour occur according to hydraulic conditions. The cause depends on a change of flows by a dune developed at the outer side. Therefore, it is very important to understand this phenomenon to prevent disasters. In this study, researchers performed a three-dimensional numerical simulation of flow in a 90° curved channel with a small width-to-depth ratio when a dune was developed at the outer side in the channel. In the model, the FAVOR method in the Cartesian coordinate system was adopted and the k-ε turbulence model was employed to predict a turbulent flow. The model was applied in a laboratory experiment, and the simulated results were compared with the experimental ones. Moreover, the reason why the scour region appeared at the inner side in the channel was indicated from the numerical results.

INTRODUCTION

Numerous studies concerning river-bed variation in river bend have been conducted in the past because the points where rivers bend are the main places where disasters tend to occur at the time of a flood. Particular attention has been paid to the bed variation in uniformly curved channels that has been examined experimentally and analytically for many years. As the experimental study, in Japan, numerous studies have been conducted after Suga (1), and these studies have mainly been carried out for a river with a large width-to-depth ratio. In recent years, several studies for a minor river with small width-to-depth ratio have been carried out. Kawai & Julien (2) conducted a laboratory experiment of bed variation using a 90° curved channel with a small width-to-depth ratio less than 10, and pointed out the possibility that a scour region would appear at the inner side in curved channels with the bed material of comparatively coarse sand. Hinokidani et al. (3) performed a laboratory experiment of detailed measurements of flows at the time of bed variation using the same conditions as Kawai & Julien (2), and the experimental results showed clearly that the inner side scour was generated by a change of flows accompanied by a development of a dune at the outer side in the channel. Furthermore, they showed clearly that a big scour hole appeared behind the dune in the outer side when the dune was formed. Thus, since the scour region at the inner side and the big scour hole at the outer side occurred according to hydraulic conditions in a curved river with small width-to-depth ratio, it is very important to understand the flow and bed variation because of disaster prevention.

On the other hand, as the analytical study of bed variation in such curved channels, the numerical simulations by 3-D model have been carried out after the rapid progress of computers in recent years. Shimizu et al. (4) conducted

the numerical simulations of the 3-D flow and bed deformation for meandering and curved open channel. Fukuoka et al. (5) calculated the 3-D flow and bed variation in curved channels with gentler bank slope. They performed calculations by means of a k-ε turbulence model. Moreover, Wu et al. (6) performed the numerical simulation for 180° curved channel. However, the past analytical studies containing these conducted under the conditions that the width-to-depth ratio is large or the ratio between flow depth and radius of curvature is small, and there are few examinations conducted on the conditions with a small width-to-depth ratio. In the case of the analytical study on the conditions that the width-to-depth ratio is small, the numerical simulation of bed variation for the experiment of Kawai & Julien (2) was carried out by Rünther & Olsen (7). The numerical results by Rünther & Olsen (7) were able to reproduce the bed topography at the equilibrium stage on the experiment as a whole. However, the scour depth at the inner side was small compared with the experimental results, and since the examinations about temporal variation of bed topography or reproducibility of flows was not conducted, it is not known whether the inner side scour was generated by the change of flows accompanied by the development of the dune at the outer side. Although detailed numerical examinations of the flow and turbulent structures in uniformly curved channels with a small width-to-depth ratio was conducted by Sugiyama, H. & Sugiyama, S. (8), the numerical simulation was performed for flat fixed bed and did not take the bed variation model into consideration in the model.

In such numerical models for curved channels, the boundary-fitted coordinate system is used widely because the coordinate system can express a river form and unevenness of river-bed and can ensure the accuracy of calculation easily ((4), (5), (6), (7), (8)). However, in the coordinate system, since the calculating points become dense or coarse when the curvature of river is large and the river form is more complicated, the accuracy of calculation may depress. In such cases, it is better to use the Cartesian coordinate system rather than the boundary-fitted coordinate system. Furthermore, in the case of the numerical simulation for an actual river, using the Cartesian coordinate system is more practical because the arrangement of mesh data of river-bed elevation becomes easy by the laser scanner survey in recent years (Matsumoto et al. (9)).

The final purpose of the present study is to develop a bed variation model which can respectively reproduce the generation of a dune, the outer local scour behind the dune and the inner scour region in curved river with a small width-to-depth ratio. Therefore, at the initial stage of this study, a numerical model which can reproduce a flow in curved channel with a small width-to-depth ratio when the dune was generated at the outer side was developed. In order to examine the validity of the model, the model was applied to the laboratory experiment by Hinokidani et al. (3) and the numerical results were compared with the experimental results.

NUMERICAL MODEL

Governing Equations

In this model, the Cartesian coordinate system was adopted, and the FAVOR method (Hirt & Sicilian (10)), which can impose the boundary conditions of curved rivers or complicated river-bed topography smoothly in the coordinate system, was introduced into the governing equations. In consideration of the practicality and the numerousness of application examples, the k-ε turbulence model was adopted for evaluation of the eddy viscosity coefficient. The governing equations into which the FAVOR method is introduced are denoted as follows:

[Momentum equation]

$$\frac{\partial u_l}{\partial t}+\frac{1}{V}\left\{\frac{\partial A_{(m)}u_m u_l}{\partial x_m}\right\}=-g\delta_{3l}-\frac{1}{\rho}\frac{\partial P}{\partial x_l}+\frac{1}{V}\frac{\partial}{\partial x_m}\left\{A_{(m)}(\nu+\nu_t)\left(\frac{\partial u_l}{\partial x_m}+\frac{\partial u_m}{\partial x_l}\right)\right\} \tag{1}$$

[Continuity equation]

$$\frac{\partial}{\partial x_m}\left\{A_{(m)}u_m\right\}=0 \tag{2}$$

[k-equation]

$$\frac{\partial k}{\partial t}+\frac{1}{V}\left\{\frac{\partial A_{(m)}u_m k}{\partial x_m}\right\}=\frac{1}{V}\frac{\partial}{\partial x_m}\left\{A_{(m)}\nu_k\frac{\partial k}{\partial x_m}\right\}+\nu_t\frac{\partial u_l}{\partial x_m}\left(\frac{\partial u_l}{\partial x_m}+\frac{\partial u_m}{\partial x_l}\right)-\varepsilon \tag{3}$$

[ε-equation]

$$\frac{\partial \varepsilon}{\partial t}+\frac{1}{V}\left\{\frac{\partial A_{(m)}u_m \varepsilon}{\partial x_m}\right\}=\frac{1}{V}\frac{\partial}{\partial x_m}\left\{A_{(m)}\nu_\varepsilon\frac{\partial \varepsilon}{\partial x_m}\right\}+C_1\frac{\varepsilon}{k}\nu_t\frac{\partial u_l}{\partial x_m}\left(\frac{\partial u_l}{\partial x_m}+\frac{\partial u_m}{\partial x_l}\right)-C_2\frac{\varepsilon^2}{k} \tag{4}$$

$$\nu_t=C_\mu\frac{k^2}{\varepsilon};\quad \nu_k=\nu+\frac{\nu_t}{\sigma_k};\quad \nu_\varepsilon=\nu+\frac{\nu_t}{\sigma_\varepsilon} \tag{5}$$

where, t = time; l = 1, 2, 3; m = 1, 2, 3; $(x_1, x_2, x_3) = (x, y, z)$ in the Cartesian coordinates (x, y and z denote the horizontal, cross and vertical coordinate respectively in this study); u_l = velocity in x_l direction; $(u_1, u_2, u_3) = (u, v, w)$; V = fractional volume rate; $A_{(m)}$ = fractional area rate in x_m direction; $(A_1, A_2, A_3) = (A_x, A_y, A_z)$; g = gravitational acceleration; δ = Kronecker's delta; ρ = fluid density; $P = p + 2/3k$; p = pressure; ν = kinematic viscosity of fluid; k = turbulent kinetic energy; ε = turbulent dissipation rate; and ν_t = eddy viscosity coefficient. The following standard values were used for each constant in the k-ε turbulence model:

$$C_\mu = 0.09;\quad \sigma_k = 1.00;\quad \sigma_\varepsilon = 1.30;\quad C_1 = 1.44;\quad C_2 = 1.92 \tag{6}$$

Numerical method

The numerical scheme was almost the same as the C-HSMAC method on the collocated grid arrangement proposed by Ushijima and Nezu (11). The definition of the calculated points on the x-y plane is shown in Fig.1. The procedure of the numerical calculation is explicated as follows: first, the pressure p was divided into the static pressure p_0 and the anomalous pressure p', and the presumed velocities in the cell center (u_c, v_c, w_c) were calculated by the momentum equations from which the anomalous pressure term was excluded. The QUCIK scheme and the Adams-Bashforth method were applied to the discretization of the momentum equations. Next, the presumed velocities on the cell boundary (u_b, v_b, w_b) were calculated by linear interpolation using the presumed velocities in the cell center (u_c, v_c, w_c), and both the new anomalous pressure p' and the new velocities on the cell boundary (u_b, v_b, w_b) were solved by the HSMAC method. Then, the new velocities in the cell center (u, v, w) were calculated from the presumed velocities in the cell center (u_c, v_c, w_c) using the central difference value of the new anomalous pressure p'. Finally, using the new velocities on the cell boundary (u_b, v_b, w_b), the new surface position was calculated by the 2D horizontal continuity equation which integrated with Eq.2 in the vertical direction. In this study, in order to ensure the conservation of mass, the 2D horizontal continuity equation was used for the calculation of the new surface position. Moreover, in consideration of the stability of calculation, the first order upwind scheme was applied to each convective term of Eqs.3 and 4.

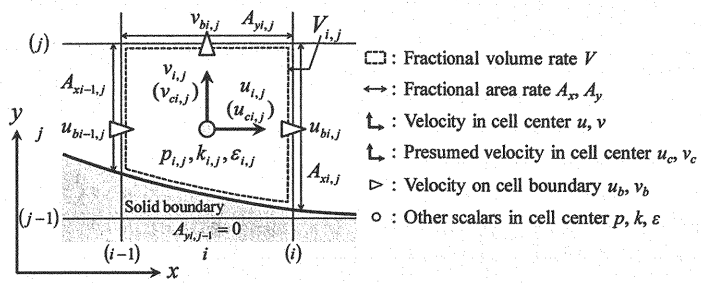

Fig.1 Definition of calculated points on *x*-*y* plane

Boundary conditions

As the upstream boundary condition, the discharge corresponding to an objective experiment was given, and the turbulent kinetic energy corresponding to 1% of the turbulent velocity of the main flow was given to the turbulent kinetic energy k. The turbulent dissipation rate ε at the upstream boundary was given so that it might be set to ν_t/ν = 10 (Kimura & Hosoda (12)). The water level measured in the experiment was given at the downstream boundary. The wall function based on the logarithmic velocity distribution and the assumption of local equilibrium of turbulence was imposed at the solid boundary. The free-slip condition for u, v and k was applied at the water surface. The dissipation rate at the water surface ε_s was given by the following formula proposed by Sugiyama et al. (13):

$$\varepsilon_s = \frac{C_\mu^{3/4} k_s^{3/2}}{\kappa z'} \tag{7}$$

where, k_s = turbulent kinetic energy at water surface; κ = Von Karman constant (= 0.41); and z' = distance from the center of the cell adjoin the water surface.

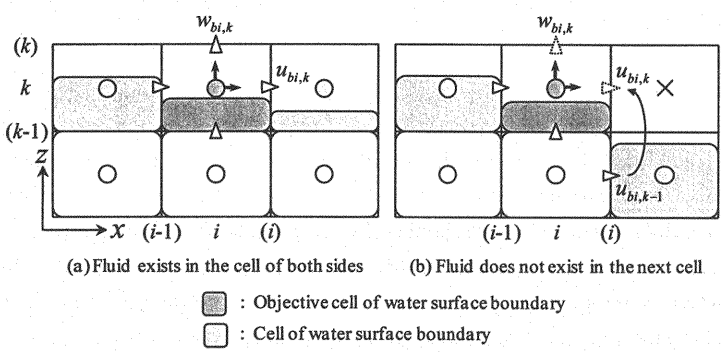

Fig.2 Treatment of the water surface

In this section, the treatment of the water surface is described in detail. The modeled water surface on the *x*-*z* plane is shown in Fig.2. In this model, as shown in Fig.2 (a), the water surface in the cell was modeled by the flat. The vertical flow velocity on the water surface boundary $w_{bi,k}$ was calculated by Eq.2. However, as shown in Fig.2 (b), when there was no fluid in the next cell, the horizontal flow velocity on the cell boundary under one $u_{bi,k-1}$ first was given to $u_{bi,k}$ in consideration of the free-slip condition. Then, the vertical flow velocity $w_{bi,k}$ was calculated by Eq.2.

As initial conditions, $u_l = 0$, $p' = 0$ and the fixed water level higher than the measured water level were given to all calculated points. Then, while the initial water level was gradually decreasing to the measured water level at the downstream boundary, the discharge gradually increased to the experimental discharge at the upstream boundary.

EXPERIMENTAL AND NUMERICAL CONDITION

Outline of objective experiment

Table 1 Experimental conditions (Hinokidani et al. (3))

Curved angle (°)	90	Mean grain size d_m (mm)	0.6
Channel width B (cm)	20	Discharge Q (ℓ/s)	4.0
Radius of curvature r (cm)	60	Mean flow depth h (cm)	4.0
Bed slope I_b	1/300	Width-to-depth ratio B/h	5.0

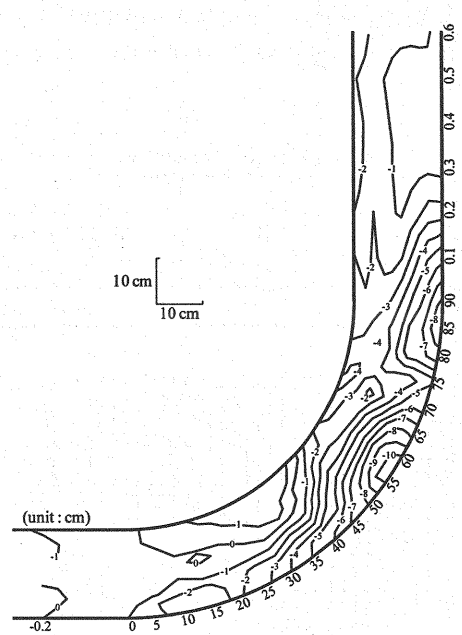

Fig.3 Observed bed contours at the time of the flow velocity measurement (Hinokidani et al. (3))

Hinokidani et al. (3) experimentally examined the characteristics of a flow and bed variation in a 90° curved channel with small width-to-depth ratio less than 10. The experimental conditions are shown in Table 1. In the experiment, the sand used for the bed material was fairly uniform, and the equilibrium sediment discharge was supplied every 5 minutes from the upstream. The measurements of bed variation at the inner and outer side in the channel were conducted. Moreover, the bed when the dune developed at the outer side was fixed. Measurements of the flow velocity were carried out. The bed contours when the flow velocity was measured is shown in Fig.3. In this figure, the crest of the dune exists at the outer side in the 75° section, and the local scour is formed near the 55° section. The scour region is formed also at the inner side near the 75° section. Hinokidani et al. (3) showed clearly that the local scour at the outer side occurred by the spiral flow generated behind the dune when the convergent main flow at the outer side submerged toward the bed. Furthermore, they showed clearly that the rapid scour advanced at

the inner side temporarily in the time zone in which the strong spiral flow was formed, and pointed out the possibility that the scour region appeared in the inner side according to hydraulic conditions. In order to reproduce both local scour at the outer side and the inner side accompanied by the development of the dune, the numerical model, which can reproduce the developed process of the spiral flow by the submergence of the main flow to the outer side, is indispensable. Therefore, in this study, the numerical simulation of a flow for the bed topography shown in Fig.3 was conducted.

Numerical condition

Table 2 and Fig.4 show the numerical conditions and the numerical grids used in this simulation respectively. Although only the curvature part is shown in Fig.4, the 70cm straight open channel was installed in the upstream and downstream region in the actual simulation. Moreover, in order to avoid the divergence of the calculation, the solid boundary cell was treated as a solid wall when the fractional volume of the solid boundary cell was smaller than 5%. Here, the cell by which the fractional volume became 5% or less was slightly in the corner where the wall intersects with the bed. Therefore, it is thought that the influence which this approximation exerts on the calculation is small. Moreover, we confirmed that the preparatory simulated results which set $\Delta x = \Delta y = 1$ cm was almost the same as the results of $\Delta x = \Delta y = 2$ cm case.

Table 2 Numerical conditions

Number of mesh	x-axis	70	Δt (sec)	0.001
	y-axis	70	$\Delta x, \Delta y$ (cm)	2.0
	z-axis	40	Δz (cm)	0.5
Flow depth at the downstream end $h_t = 4.0$ cm, Manning roughness $n = 0.014$				

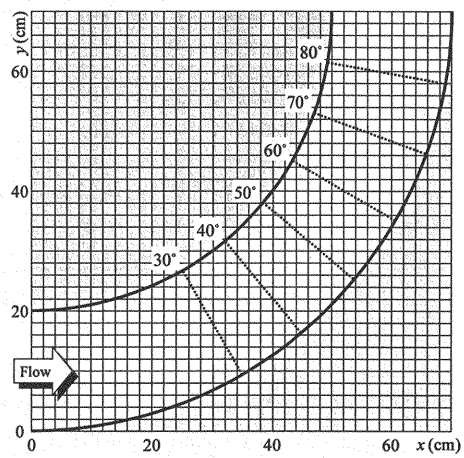

Fig.4 Numerical grids in x-y plane

RESULTS AND DISCUSSION

In the following sections, comparisons of the flow velocity profiles etc. in each transverse section of the dotted line shown in Fig.4 are drawn. However, since the Cartesian coordinate system was adopted in this numerical model,

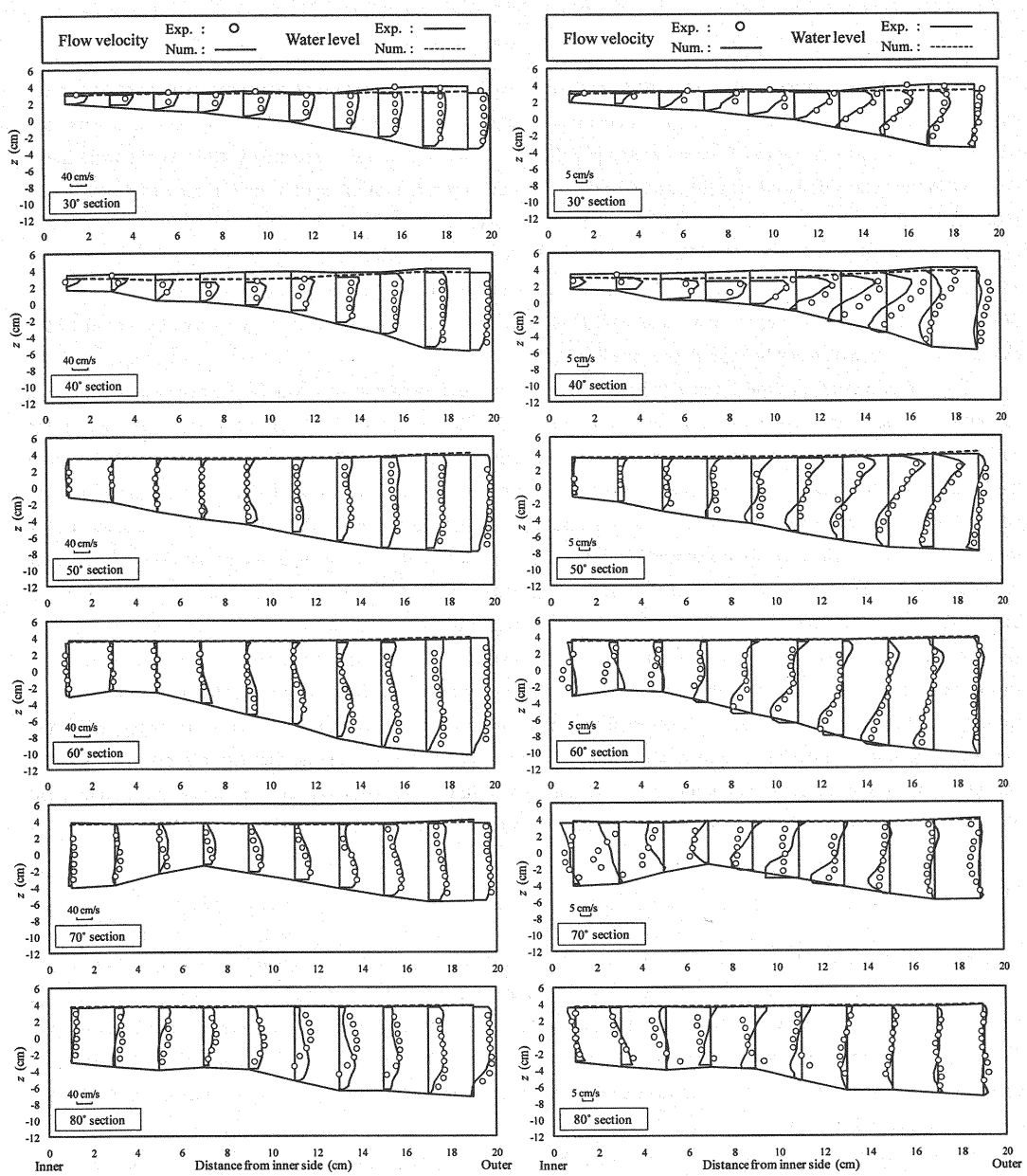

(a) Longitudinal velocity profiles (b) Transverse velocity profiles

Fig.5 Comparisons of flow velocity profiles in transverse section

(Exp. : experimental results; Num.: numerical results)

the calculated points and the measured points of flow velocity in the experiment cannot be completely made coincidentally. Therefore, for the numerical results, the interpolated values from the calculated flow velocity near the measured points are shown.

Velocity profiles in transverse section

Fig.5 shows comparisons of flow velocity profiles in each transverse section between the experimental and the numerical results. From these figures, the numerical results are in agreement with the experimental results as a whole. In the upstream region from outer scour hole (= 60° section), a same secondary flow as the experiment occurred at the outer side [see Fig.5 (b)], and a back flow by the separation of the main flow is reproduced at the inner side [see Fig.5 (a)]. At the center of the channel in the 50° section, a submergence of the main flow toward the bed can be reproduced [see Fig.5 (a)]. On the other hand, in the downstream region from the outer scour hole, an acceleration of the flow near the bed by the collision to the dune of the main flow can be seen in the 70° section. Moreover, in the scour hole at the inner side (= 70°~80° sections), a weak secondary flow toward the center of the channel near the bed also can be reproduced [see Fig.5 (b)].

Thus, this numerical model can reproduce the flow in the experiment as a whole. However, although the separation of the main flow from the inner side occurs at the 40° section in the experiment, the separation in the simulation occurred at the downstream lower than the experimental results. This situation is understood also from the horizontal velocity vectors shown in the next section. As the result, the calculated water surface profiles at the 40° section are not in agreement with the observed results. In addition, a start on the submergence of the main flow toward the outer scour hole is slow compared with the experimental results, and the increase of the flow velocity near the bed in the outer scour hole in which the maximum scour depth occurs (= 60° section) cannot be reproduced. Therefore, when the numerical model is applied to a simulation of bed variation, the maximum scour depth at the outer side may be evaluated as small at the present stage. Moreover, in the downstream region from the outer scour hole, an increase of the transverse velocity near the bed due to the effect of the dune appears in the inner side direction strongly and the flow reaches near the water surface in the inner side. It is thought that the reason for this is that the flow submerged toward the bed is turned in the inner side direction by the dune before the flow reaches the outer side enough when the start on the separation is slow. Consequently, improvements still need to be made in the model, and it is necessary to study the factors which cause the main flow to submerge toward the bed.

Horizontal velocity vectors

Fig.6 shows horizontal velocity vectors obtained from (a) the experimental results and (b) the numerical results respectively. In the experimental results, the separation of the main flow occurs at the inner side near the 40° section, and the flow concentrates toward the outer side near the 55° section in which the maximum scour depth occurs [see Fig.6 (a)]. Moreover, the back flow region is formed in the inner side, and the flow concentrated in the outer side spreads toward the inner side at the downstream from the 55° section, especially, the spreading tendency appears notably near the bed.

On the other hand, in the numerical simulation, the formation of back flow region by separation of the main flow, the concentration of the main flow in the outer side and the spreading tendency of the flow toward the inner side becoming strong near the bed can be reproduced [see Fig.6 (b)]. These simulated results are almost same as the experimental results. Furthermore, the flow direction near the side wall is smoothly expressed along the channel by introducing the FAVOR method. However, as aforementioned, the start position of the separation of the main flow is located at the lower reach compared with the experimental results, and the flow velocity at the inner side just before the separation (= 40° section) is very large. Also, the size of back flow region is slightly smaller compared with the experiment. In order to improve the flow regime, although the examination by means of a 0-equation model or the examination by a given high wall roughness etc. was attempted in the preparatory simulation, but it was not improved. The influences due to effect of the FAVOR method, by the boundary conditions on the side wall or by the wall

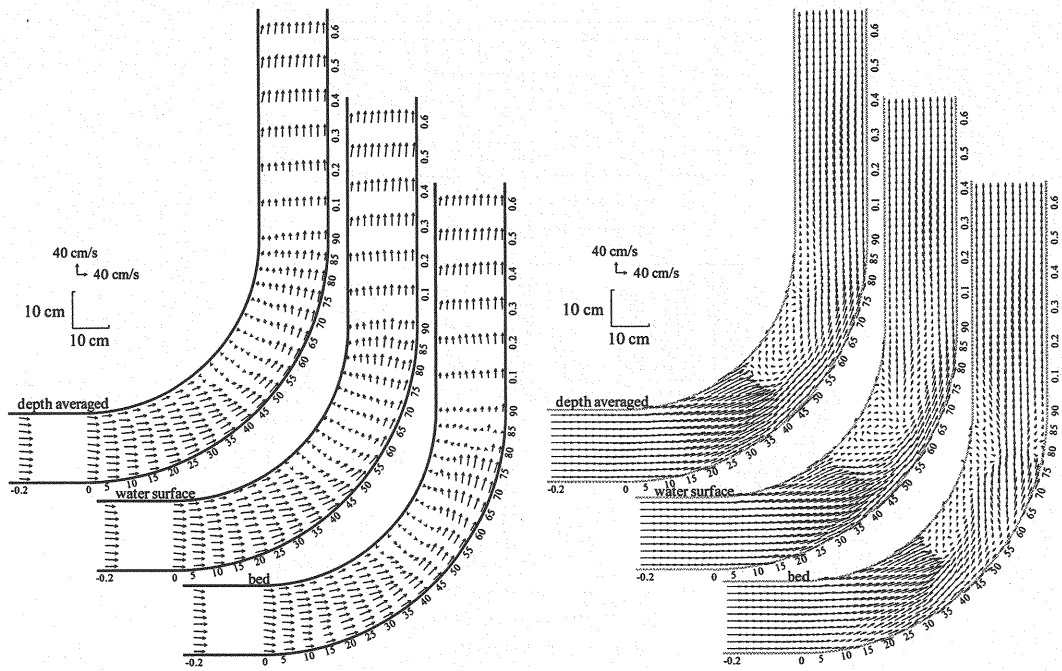

(a) Experimental results (b) Numerical results

Fig.6 Horizontal velocity vectors

function etc. can be considered as the main causes. Moreover, the influence by the k-ε model which assumed the isotropy of turbulence can be also considered. But such causes cannot be understood clearly at the present stage. In order to reproduce the outer local scour by the submergence of the main flow toward the bed with sufficient accuracy, it is very important to predict the location of the separation correctly. Therefore, it is necessary to investigate the above problems in detail in the future.

Longitudinal velocity vectors

Fig.7 shows longitudinal velocity vectors in the outer side achieved from (a) the experimental results and (b) the numerical results. In the experiment, a downward flow toward the scour hole occurs at the upstream region from the outer scour hole and the flow velocity below the half of flow depth increases at the 45°~60° sections [see Fig.7 (a)]. An upward flow behind the dune appears clearly at the downstream region from the outer scour hole. In the numerical simulation, since the submergence of the main flow is slow due to the delay of the inner side separation, the increase of the flow velocity below the half of flow depth cannot be reproduced at the 45°~60° sections in the 3cm longitudinal section from the outer side [see Fig.7 (b)]. However, the downward flow toward the scour hole can be reproduced. In the 5 cm longitudinal section from the outer side, the increase of the flow velocity below the half of flow depth can be reproduced simultaneously with the downward flow toward the scour hole, and the upward flow behind the dune also can be reproduced.

Transverse flow regime and inner side scour

The generated process of the inner side scour which clearly shown in the experiment conducted by Hinokidani et al. (3) can be described as follows: first, the direction of the main flow turned to the inner side, which was caused by

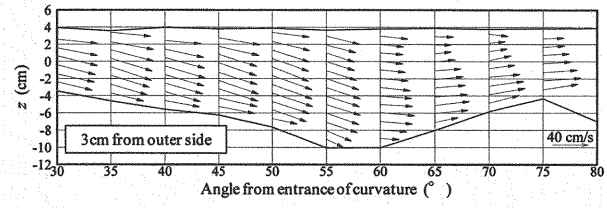

(a) Experimental results

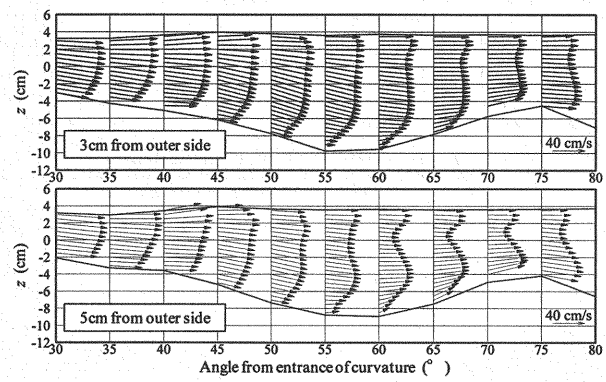

(b) Numerical results

Fig.7 Longitudinal velocity vectors in outer side

the spiral flow generated in the scour hole of the outer side. Next, the same spiral flow as the outer spiral flow was generated in the inner side by the collision to the inner side of the main flow. Finally, the inner spiral flow scoured out the inner side bed and the inner side scour occurs. As aforementioned, in the numerical results, the secondary flow at the outer side and the weak secondary flow at the inner side were reproduced. A discussion of the flow when the inner side scour occurs is added from the numerical results.

Fig.8 shows velocity vectors in each transverse section. These figures depict that in the upstream region from the outer scour hole (= 60° section), the strong downward flow which flows toward the scour hole occurs at the outer side, and the secondary flow which flows toward the inner side near the bed occurs. In particular, the strong upward flow occurs near the bed in the 60° section in which the maximum scour depth is developed. It is thought that the outer spiral flow is composed of these flows.

On the other hand, in the downstream region from the outer scour hole, the strong inflow near the outer side bed by the influence of the dune flows into the inner side scour. Also, the weak secondary flow which flows toward the outer side near the bed is formed by the inflow. Here, because the main flow did not reach the inner side enough in the experiment conducted by Hinokidani et al. (3), the clear spiral flow accompanied by the upward flow near the inner side bed cannot be reproduced in the simulation. However, if the main flow reaches the inner side enough, that is, if the inflow flux from the outer side to the inner side increases because of sufficient submergence of the main flow into the outer scour hole, the strong spiral flow will be generated in the inner side. As the result, it is thought that the inner side scour occurs due to the inner side spiral flow.

CONCLUSION

In this study, a numerical simulation of a flow in uniformly 90° curved channel with small width-to-depth ratio when a dune developed was performed. In the model, the Cartesian coordinate system was adapted, and the FAVOR method was introduced into the governing equations. According to a comparison of the experimental results and the

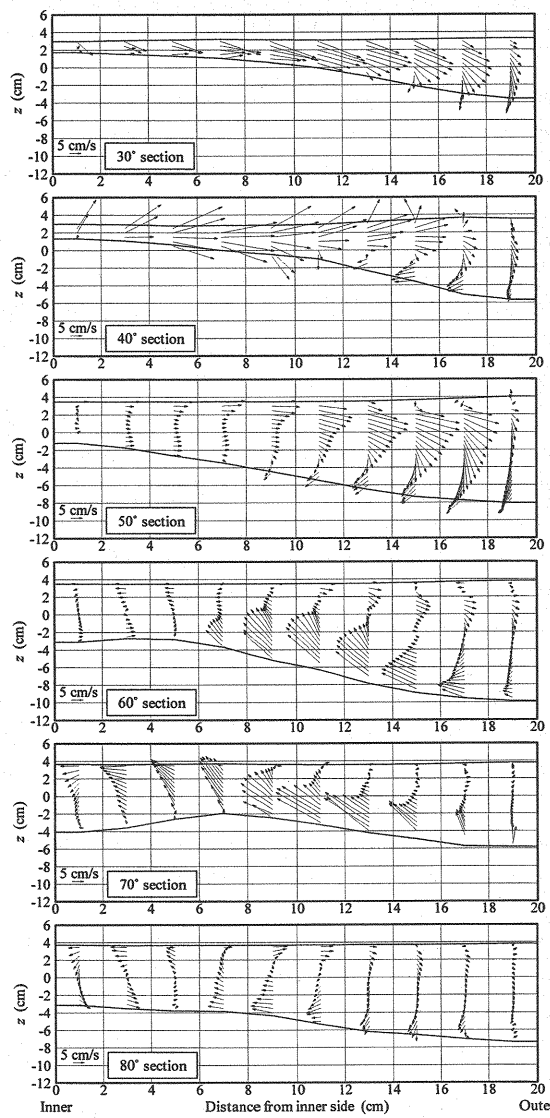

Fig.8 Velocity vectors in each transverse section

numerical results, the numerical model can reproduce the flow in the curved channel with small width-to-depth ratio, especially, the flow regime that the main flow after the separation submerges toward the bed of scour hole in the outer side was able to be reproduced. Moreover, the flow direction near the side wall was able to be expressed smoothly by introducing the FAVOR method. However, the location of the separation was not able to be reproduced, and its influenced factors cannot be confirmed. Furthermore, the flow regime when the inner side scour occurs was discussed according to the numerical results. It can be surmised that the inner side scour is generated by the inner side spiral flow formed by the strong flow from the bed of the outer side spiral flow. In the future, the reproducibility of the location of the separation and the bed variation model should be examined.

REFERENCES

1. Suga, K. : Stable bed topography in curved open channel (Part 2), *Proc. of the 10th Japanese Conference on Hydraulics*., pp.111-116, 1996 (in Japanese).
2. Kawai, S. and Julien, P. Y. : Point bar deposits in narrow sharp bends, *Journal of Hydraulic Research*, Vol.34, No.2, pp.205-218, 1996.
3. Hinokidani, O., Michiue, M. and Kawai, S. : Experimental study on bed variation and sand waves in curved channels, *Annual Journal of Hydraulic Engineering*, JSCE, Vol.42, pp.979-984, 1998 (in Japanese).
4. Shimizu, Y., Yamaguchi, H. and Itakura, T. : Three-dimensional computation of flow and bed deformation, *Journal of Hydraulic Engineering*, ASCE, Vol.116, No.9, pp.1090-1180, 1990.
5. Fukuoka, S., Nishimura, T. and Sannomiya, T. : Flow and bed profiles in curved channels with gentler bank slopes, *Journal of Hydraulic, Coastal and Environmental Engineering*, No.509/II-30, pp.155-167, 1995 (in Japanese).
6. Wu, W., Rodi, W. and Wenka, T. : 3D numerical modeling of flow and sediment transport in open channels, *Journal of Hydraulic Engineering*, ASCE, Vol.126, No.1, pp.4-15, 2000.
7. Rüther, N. and Olsen, N. R. B. : Three-dimensional modeling of sediment transport in a narrow 90° Channel Bend, *Journal of Hydraulic Engineering*, ASCE, Vol.131, No.10, pp.917-920, 2005.
8. Sugiyama, H. and Sugiyama, S. : Numerical study on turbulent structure in curved open channel with roughness wall, *Journal of Hydraulic, Coastal and Environment Engineering*, No.747/II-65, pp.71-83, 2003 (in Japanese).
9. Matsumoto, K., Nagura, H., Tamaki, H., Kobatake, S., Shimizu, Y. and Akiyama, K. : Field measurement of 3-dimensional shape of the landform of river bed of Kinu river by using 3D laser scanner, *Advances in River Engineering*, Vol.9, pp.253-258, 2003 (in Japanese).
10. Hirt, C. W. and Sicilian, J. M. : A porosity technique for the definition obstacle in rectangular cell meshes, Flow Science, Inc. Los Alamos, New Mexico, pp.450-469, August 1985.
11. Ushijima, S. and Nezu, I. : Computational method for free-surface flows on collocated grid with moving curvilinear coordinates, *Journal of Hydraulic, Coastal and Environmental Engineering*, No.698/II-58, pp.11-19, 2002 (in Japanese).
12. Kimura, I. and Hosoda, T. : Numerical analysis of flows around square cylinder by means of non-linear k-ε model, *Annual Journal of Hydraulic Engineering*, JSCE, Vol.43, pp.383-388, 1999 (in Japanese).
13. Sugiyama, H., Akiyama, M. and Matsubara, T. : Numerical simulation of compound open channel flow on turbulence with a Reynolds stress model, *Journal of Hydraulic, Coastal and Environmental Engineering*, No.515/ II-31, pp.55-65, 1995 (in Japanese).

APPENDIX – NOTATION

The following symbols are used in this paper:

$A_{(m)}$ = fractional area rate in x_m direction;

B = channel width;

B/h = width-to-depth ratio;

d_m = mean grain size;

g = gravitational acceleration;

h = mean flow depth;

h_t = flow depth at downstream end;

I_b = bed slope;

k = turbulent kinetic energy;

k_s = turbulent kinetic energy at water surface;

n = Manning roughness;

p = pressure;

p' = anomalous pressure;

Q = discharge;

r = radius of curvature;

t = time;

u_i = velocity in x_i direction;

V = fractional volume rate;

z' = distance from cell center adjoin water surface;

δ = Kronecker's delta;

ε = turbulent dissipation rate;

κ = von Karman constant;

ν = kinematic viscosity of fluid;

ν_t = eddy viscosity coefficient; and

ρ = fluid density.

(Received Jul, 15, 2009 ; revised Apr, 16, 2010)